Proceedings of the
Annual Stability Conference
Structural Stability Research Council
Louisville, Kentucky, April 1-4, 2025

Optimum web stiffener for the buckling stability of web perforated cold-formed steel storage rack columns

Amoke Shabhari[1], Vijaya Vengadesh Kumar Jeyapragasam[2]

Abstract
Storage rack structural systems have occupied a remarkable share of the global market due to the demanding logistics operations. Uprights are the primary compression member that controls the overall stability of the rack system. For a sustainable structural system, moving towards maximum material utilization, there is increasing research on the cross-section optimization of storage rack uprights, while maintaining the limit state stability at cross-section as well as member level. The current article presents the results from an ongoing experimental research work, addressing the effect of web stiffener in the local buckling of cold-formed steel (CFS) rack uprights in the presence of patterned web perforations throughout the length. Finite element numerical models of the simple rack and lipped rack sections are carefully validated using tested specimens, and an extensive parametric study which includes various web-to-flange width ratios and non-dimensional slenderness ratios is conducted to cover a wide range of web stiffener size, shape, and included angle. The columns are subjected to concentric compression load with fixed end supports. The objective of the study is to encourage practitioners to optimally design the web stiffener of CFS web perforated columns utilizing the local post-buckling reserve strength due to the presence of the web stiffeners. Further, the study examines the accuracy of the well-established DSM-based strength predictions for the wide range of local non-dimensional slenderness ratios, in the presence of web stiffener and web perforations, which allows simpler reiterative design procedures.

1. Introduction

The cold-formed steel (CFS) members are widely preferred in construction industries owing to their superior strength-to-weight ratio, installation convenience, and versatility to form various cross-sectional shapes and sizes. Due to their high-element slenderness and open cross-section, these members can undergo local, distortional, and global or any possible interaction among these buckling modes, depending on the cross-section geometry, boundary, and loading conditions, resulting in failure of geometry before material. The post-buckling reserve strength of local buckling is higher whereas it is not significant for distortional and global buckling failure modes. The local buckling and post-buckling reserve strength may be further increased by adding stiffeners in the cross-sections. An analytical method to determine the local buckling capacity of the CFS columns was proposed by Kalyanaraman (1979). The influence of shift in effective centroid in pinned support condition in CFS columns failing in local buckling was studied by Young and Rasmussen (1998). The mutual interaction between the buckling modes always shows lower capacity than independent buckling failures. (Camotim et al. 2020). The interaction of local and distortional buckling modes was reported in various studies (Chen et

[1] Doctoral Research Scholar, National Institute of Technology Karnataka, Surathkal, India, <amokeshabhari@gmail.com>
[2] Assistant Professor, National Institute of Technology Karnataka, Surathkal, India, <vj@nitk.edu.in>

al. 2020; Huang et al. 2021; Kwon et al. 2009; Kwon and Hancock 1992; Loughlan et al. 2012; Martins et al. 2015; Young et al. 2013).

CFS members are widely used in storage rack structures. The storage rack uprights are the columns primarily resisting axial compression and provided with a pattern of perforations across the web and flanges to permit beam-to-column connections and column-to-column bracings at different heights. These perforations enable simple and quick assembly of rack systems and flexibility in changing storage height requirements. However, the presence of such perforation affects the behavior and capacity of the CFS columns. Recent studies have emphasized the importance of perforation influence in the strength prediction of CFS columns (Shabhari et al. 2024; Francis et al. 2024; Neiva et al. 2018; Baldassino et al. 2019; Vijayavengadesh Kumar and Arul Jayachandran 2016; Zhao et al. 2017; Pu et al. 1999) The effect of discrete holes in the cold-formed steel columns may not be the same as the effect of patterned perforated holes (Smith and Moen 2014). The local buckling load would be significantly affected if the web contains two or more adjacent holes. Whereas the reduction is not significant if the web contains a discrete hole (Nedelcu 2014). The location and configuration of the perforation are significant for the columns with moderate local buckling slenderness (Shabhari et al. 2024). Various analytical design procedures to account for the effect of patterned web perforation in the columns have been developed and modified in recent years.

Even though the Effective Width Method (EWM) is the most common design method for members failing in local buckling, design calculations are cumbersome and complex. As an alternate design, the Direct Strength Method (DSM) (Schafer 2002) gained quick popularity and widely accepted due to its simple but powerful strength estimation using non-iterative and gross cross-section property based design. The DSM has been included in the North American specification and expanded for many precluded cross-sections (AISI S100 2016). The DSM was extended to design the perforated columns (Moen and Schafer 2011). Further, in recent studies, there have been investigations that examined the accuracy of DSM predictions for the perforated CFS columns. (Yao and Rasmussen 2017; Zhang and Alam 2022, 2023). The web-to-flange ratio of the cross-section (aspect ratio) is an unavoidable parameter in the DSM local buckling strength equation. Still, it is not accounted for either in the non-dimensional local buckling slenderness ratio or directly in local buckling strength calculations. Hence, a modification in the DSM (MDSM) was proposed by (Kumar and Kalyanaraman 2013) to account for the web-to-flange ratio in local buckling strength equations for stiffened lipped channel cross-sections and further extended to unstiffened plain channel sections. The MDSM local buckling strength equations were extended to account for web perforations in CFS plain channel (Francis et al. 2024) and in lipped channel columns (Shabhari et al. 2024).

Despite many advancements and improvements that have been made in the analytical design procedures, the current static storage rack design is based either on Finite Element Analysis (FEA) or experimental test procedures to design the uprights as per (BS EN 15512:2020 2020). However, the higher computational efforts for FEA and higher cost for physical testing always limit the designers to narrow down the scope of optimizing the CFS cross-sections. The CFS columns are often provided with web stiffeners to reduce the web element slenderness of the cross-section. Therefore, the local buckling capacity can be improved by providing effective web stiffeners, but at the same time, the effectiveness of the web stiffeners is a subject matter with the presence of web perforations. The inclusion of web stiffeners would significantly increase the material consumption but with the advantage of considerable increase in the post-

local buckling reserve strength, the cross-section can be optimized through the the right choice of web stiffener shape, size, and included angle.

This article examines the influence of web stiffener in local buckling strength predictions for simple and lipped rack sections having web perforations through a systematic experimental and comprehensive FE analysis. These fixed support stub column cross-sections were configured to undergo pure local buckling without any interaction with distortional and global buckling modes. The experimentally validated numerical procedures were utilized to perform an extensive parametric study covering a wide range of web-to-flange ratios, non-dimensional local buckling slenderness, and different shape, size, and included angles of web stiffeners. The influence of web stiffener on the local buckling strength of web-perforated CFS rack section is evaluated and the accuracy of existing DSM and MDSM design equations are assessed.

2. Design equations for local buckling of CFS columns

The local buckling strength equations are presented below and the details of variables are presented in the nomenclature at the end.

2.1 For unperforated columns

2.1.1 Direct Strength Method (Schafer 2002)

$$P_{nL} = P_y \quad \text{for} \quad \lambda_L \leq 0.776 \quad (1)$$

$$P_{nL} = \left[1 - 0.15\left(\frac{P_{crl}}{P_y}\right)^{0.4}\right]\left[\left(\frac{P_{crl}}{P_y}\right)^{0.4}\right]P_y \quad \text{for} \quad \lambda_L > 0.776 \quad (2)$$

$$\lambda_L = \sqrt{\frac{P_y}{P_{crL}}}$$

2.1.2 Modified Direct Strength Method (Kumar and Kalyanaraman 2013)

$$\frac{P_{ul}}{P_y} = 1 \quad \text{for} \quad \lambda_L \leq 0.60 \quad (3)$$

$$\frac{P_{ul}}{P_y} = \left[1 - \alpha_1\left(\frac{P_{crl}}{P_y}\right)^{\beta}\right]\left(\frac{P_{crl}}{P_y}\right)^{\beta} \leq \frac{P_{ul,max}}{P_y} \quad \text{for} \quad \lambda_L > 0.60 \quad (4)$$

$$\frac{P_{ul,max}}{P_y} = \left[1 - 0.12\left(\frac{P_{crl}}{P_y}\right)^{0.15}\right]\left(\frac{P_{crl}}{P_y}\right)^{0.15} \quad \text{for} \quad \frac{h}{b} \geq 1.00 \quad (5)$$

$$\frac{P_{ul,max}}{P_y} = \left[1 - 0.2\left(\frac{P_{crl}}{P_y}\right)^{0.32}\right]\left(\frac{P_{crl}}{P_y}\right)^{0.32} \quad \text{for} \quad \frac{h}{b} < 1.00 \quad (6)$$

$$\alpha_1 = 0.27(2 - \mu)$$

$$\beta = \frac{1}{100}(50 - 7\mu) \geq 0.35$$

$$\mu = max\left[\frac{h}{b}, \left(\frac{b}{h}\right)^{0.6}\right]$$

Note: All variables are defined in the Nomenclature section.

2.2 For perforated columns

2.2.1 Direct Strength Method (DSM_holes) (Moen and Schafer 2011)

$$P_{nle} = P_{ne} < P_{y,net} \quad \text{for} \quad \lambda_{le} \leq 0.776 \quad (7)$$

$$P_{nle} = \left[1 - 0.15\left(\frac{P_{crl-h}}{P_{ne}}\right)^{0.4}\right]\left[\left(\frac{P_{crl-h}}{P_{ne}}\right)^{0.4}\right] P_{ne} < P_{y,net} \quad \text{for} \quad \lambda_{le} > 0.776 \quad (8)$$

$$\lambda_{le} = \sqrt{\frac{P_{ne}}{P_{crL-h}}}$$

2.2.2 Modified Direct Strength for holes (MDSM_holes) (Shabhari et al. 2024)

$$\frac{P_{ul}}{P_y} = 1 \leq \frac{P_{y,net}}{P_y} \quad \text{for} \quad \lambda_L \leq 0.60 \quad (9)$$

$$\frac{P_{ul}}{P_y} = \min\left(\left[1 - \alpha_1\left(\frac{P_{crl}}{P_y}\right)^{\beta}\right]\left(\frac{P_{crl}}{P_y}\right)^{\beta}, \frac{P_{ul,max}}{P_y}, \frac{P_{y,net}}{P_y}\right) \quad \text{for} \quad \lambda_L > 0.60 \quad (10)$$

$$\frac{P_{ul,max}}{P_y} = \left[1 - 0.12\left(\frac{P_{crl}}{P_y}\right)^{0.15}\right]\left(\frac{P_{crl}}{P_y}\right)^{0.15}\left(\frac{P_{y,net}}{P_y}\right) \quad \text{for} \quad \frac{h}{b} \geq 1.00 \quad (11)$$

$$\frac{P_{ul,max}}{P_y} = \left[1 - 0.2\left(\frac{P_{crl}}{P_y}\right)^{0.32}\right]\left(\frac{P_{crl}}{P_y}\right)^{0.32}\left(\frac{P_{y,net}}{P_y}\right) \quad \text{for} \quad \frac{h}{b} < 1.00 \quad (12)$$

$$\alpha_1 = 0.27(2 - \mu)$$

$$\beta = \frac{1}{100}(50 - 7\mu) \geq 0.35$$

$$\mu = max\left[\frac{h}{b}, \left(\frac{b}{h}\right)^{0.6}\right]$$

$P_{y,net} = A_{net} \times f_y$,

$P_y = A_g \times f_y$

Note: All variables are defined in the Nomenclature section.

3. Experimental study

3.1 Specimen Details

A total of 8 specimens were chosen, of which 4 specimens consist of simple rack and lipped rack sections with and without web stiffeners, and 4 specimens consist of web perforated simple rack and lipped rack with and without web stiffeners. The specimens are labeled as SR for simple rack, LR for lipped rack, WSSR for web stiffened simple rack, and WSLR for web stiffened lipped rack. G refers to a solid gross section with no web perforation and P refers to a web perforated section. The measured geometric details of the specimens are shown in Table 1 and the schematic cross-sectional view of all the specimens is shown in Fig. 1. All the specimens were manufactured by press braking of cold-formed hot rolled sheets. The dimensions of the rack specimens were selected in such a way that they fail only after local buckling. The web perforation considered was trapezoid with a cross-sectional area of 200 mm^2. The trapezoid shape, oriented at 90°, was selected to represent the worst-case combination of perforation shape and orientation, as it has the greatest impact on reducing the local buckling capacity among the idealised perforation patterns (Shabhari et al. 2024). The geometry of the perforation is shown in Fig. 2. The length of all specimens was set to be three times the critical half-wavelength or three times the width of the largest plate element in the

cross-section, whichever is maximum. This was implemented to avoid the influence of end boundary conditions on the local buckling capacity of the stub columns.

Table 1: Geometric details of the tested specimens (all dimensions are in mm)

S. No.	Specimens	Thickness (t)	Web (h)	Flange (b_f)	Rear flange (b_r)	Flange Stiffener (d_f)	Web Stiffener (d_w)	Lip (d)	Length (L)
1	SR - G	1.59	99.40	75.08	23.43	20.00	-	-	298.90
2	SR - P	1.59	100.38	74.90	23.16	20.00	-	-	299.90
3	LR - G	1.59	120.26	89.64	28.26	24.00	18.00	-	359.00
4	LR - P	1.59	120.12	89.62	28.12	24.00	18.00	-	360.00
5	WSSR - G	1.59	100.12	74.83	23.57	20.00	-	10.01	298.73
6	WSSR - P	1.59	99.75	75.01	23.49	20.00	-	8.91	299.95
7	WSLR - G	1.59	120.77	90.03	28.51	24.00	18.00	11.60	359.08
8	WSLR - P	1.59	119.28	90.35	28.31	24.00	18.00	11.85	359.98

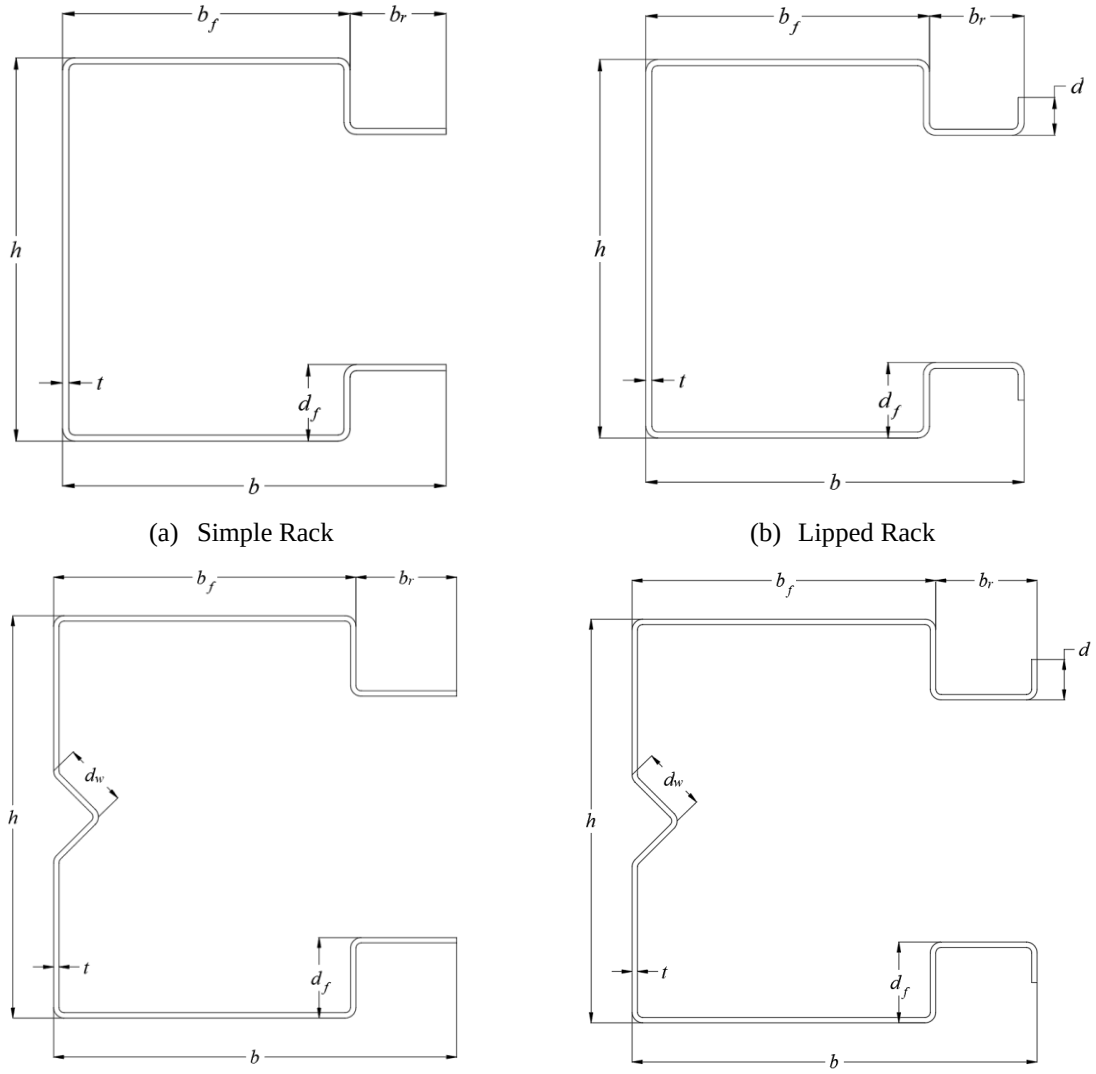

(a) Simple Rack (b) Lipped Rack

(c) Web Stiffened Simple Rack (d) Web Stiffened Lipped Rack

Figure 1: Cross-section of the specimens

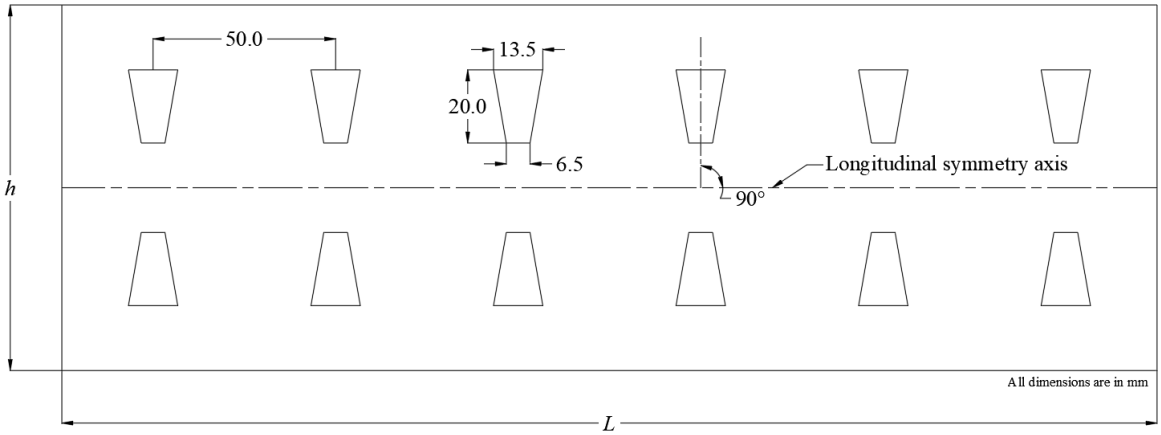

Figure 2: Geometry of Perforation

3.2 Tensile coupon test

The tensile coupon test was performed to characterize the material properties. The entire test was carried out conforming to the ASTM E8 (ASTM E8/E8M-16a 2016). The dimensions of the coupon specimens are shown in Fig. 3. The coupon specimens were laser cut from the cold-formed members. To account for the bending residual stresses in material properties, strain gauges of 5 mm gauge length and 120-ohm resistance were attached as aligned to the longitudinal axis at the center of the coupon on both sides, as shown in Fig. 4. The test was performed in 250 kN MTS servo-hydraulic UTM (Shown in Fig. 5) at the Central Research Facility in the National Institute of Technology Karnataka, India. The displacement-controlled loading at the 1 mm/min rate was applied until the specimen failed. The NI-9219 data acquisition module was used to record the strain data. The load and cross-head movement data were recorded from the machine. All data sampling was done at the rate of 20 data per second. The obtained results from the test are shown in Table 2 and the stress-strain curves are shown in Fig. 6.

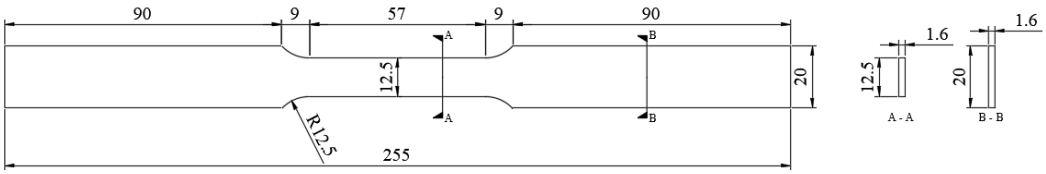

Figure 3: Geometry of tensile coupon specimens

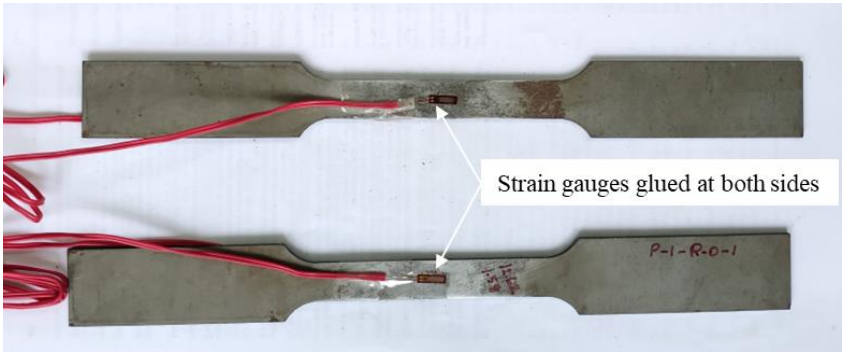

Figure 4: Coupon specimens with strain gauges attached

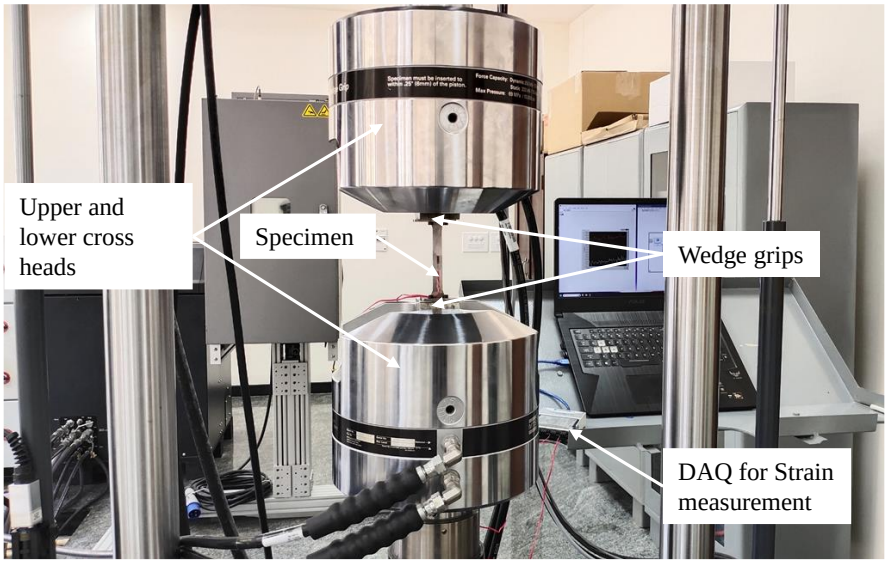

Figure 5: Experimental setup for coupon test

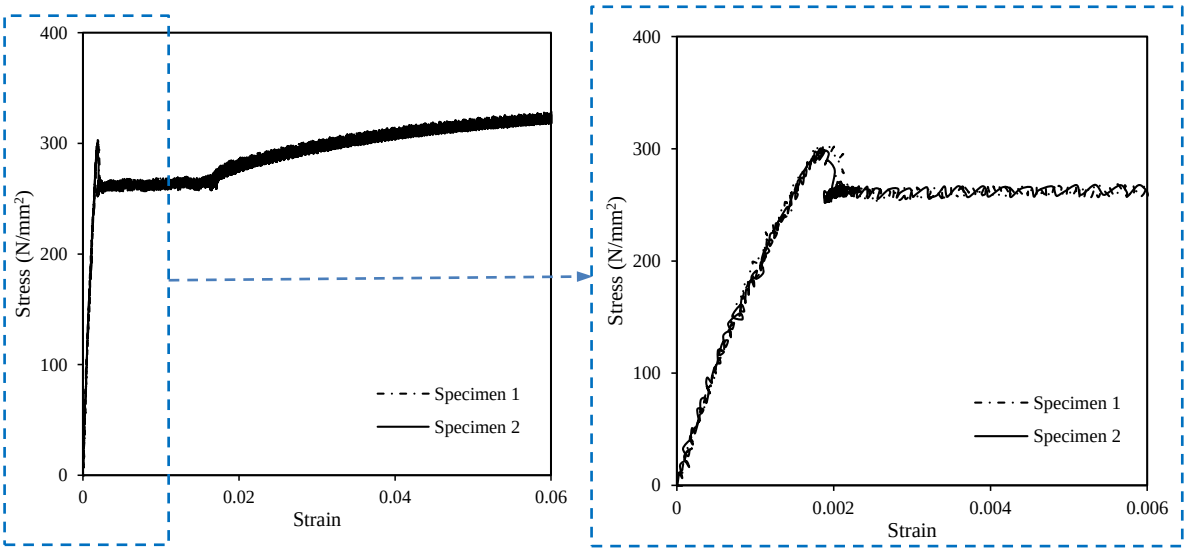

Figure 6: Measured stress and strain from tensile coupon test

Table 2: Material properties from tensile coupon test

Specimen No.	Young's modulus (E)	Yield stress (f_y)	Ultimate stress (f_u)
	(N/mm^2)	(N/mm^2)	(N/mm^2)
1	2.08×10^5	264.80	342.61
2	2.06×10^5	264.00	339.60

3.3 Stub column test

All the stub columns were tested in a 100T loading frame at the NABL-accredited Structural Testing Laboratory, established storage rack testing in M/s Craftsman Automation Limited, Pune, India. The specimens were welded with 170 mm × 170 mm square end plates at both the top and bottom, ensuring the alignment of the specimen gross section centroid with that of the plate. The end plates help in even stress distribution across the cross-section. The load setup of the stub column test is shown in Fig. 7. The load from the hydraulic cylinder was applied through the pressure pad and fastened with the top-end plate of the specimen. The torsion of the specimen was restrained by additional side clamps provided at the top and bottom, whereas

the end plates restrained the warping. The bottom setup houses a spherical steel ball bearing to ensure the proper vertical alignment of the specimen. Further, the specimen rotation about both axes of the cross-section was restrained using four corner bolts with a nominal preload of 0.5 kN. A 1000 kN high-precision HBM branded load cell was used to measure the applied load beneath the bottom plate. The loading rate was maintained as ram movement of 2 mm/min until the specimen failure. HBM branded, high precision LVDTs of 50 mm range were utilized in the experiments. Three LVDTs were placed vertically beneath the top end plates to measure axial shortening, and three LVDTs were placed horizontally to measure the transverse displacement of the web and both the flanges, as shown in Fig. 7.

3.4 Test results and discussions

It was observed that all the specimens failed by pure local buckling of the web and flanges. A buckling failure of a typical section is shown in Fig. 8, where a simultaneous buckling of the web and flanges was observed, and the ultimate capacities of all the specimens are shown in Table 3. There was no noticeable distortional and global buckling interaction during the local buckling failure. The specimens without web stiffeners, such as SR and LR, failed by simultaneously buckling of web and flanges, in which the buckling was initiated in the web due to its higher element slenderness. Web stiffened specimens of WSSR and WSLR, the presence of stiffeners at the web led to the initiation of local buckling in the flanges following the web buckling to maintain the rotation compatibility at the web-flange junction. The ultimate capacity of unperforated and perforated specimens proves that the presence of web stiffener increases the normalized local buckling strength (P_{ul} / P_y) for the same non-dimensional local slenderness ratio (λ_L). Nevertheless, this enhancement in local buckling strength with the addition of a web stiffener is minimal for perforated members due to the weak web element in the presence of perforation.

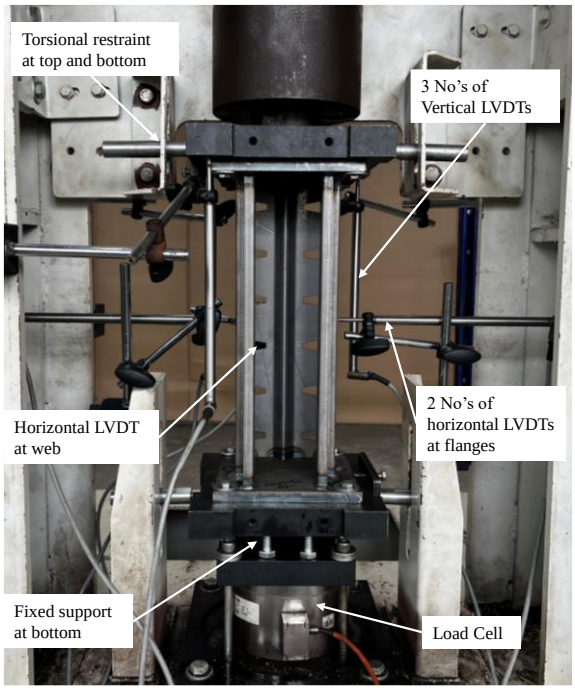

Figure 7: Loading setup and instrumentation

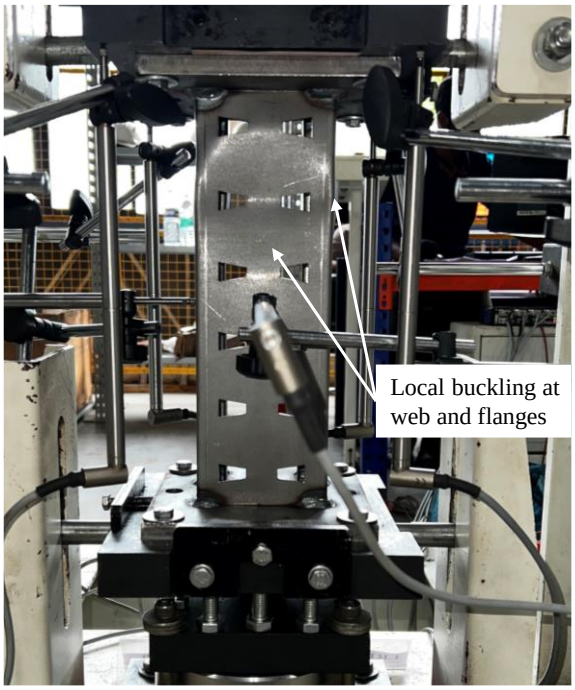

Figure 8: Buckling failure of a typical specimen

Table 3: Results from the stub column test

S. No.	Specimens	Ultimate load (P_{ul}) (kN)	λ_L	P_{ul} / P_y
1	SR - G	119.16	1.00	0.86
2	SR - P	99.78	0.98	0.82
3	LR - G	133.45	0.88	0.78
4	LR - P	134.73	0.91	0.87
5	WSSR - G	142.63	1.01	0.98
6	WSSR - P	93.85	1.00	0.75
7	WSLR - G	156.29	0.88	0.87
8	WSLR - P	125.64	0.92	0.77

4. Numerical study

4.1 Validation of the numerical model

The FE analysis is done to extend the study numerically to cover the wide range of parameters such as web-to-flange ratio, non-dimensional slenderness ratio, and size, shape, and angle of web stiffeners. Hence, to validate the numerical FE procedure, the experimental results are utilized. The ABAQUS software was used to perform the FE analysis. The 3D extruded shell element was employed to model the columns. The numerical study was conducted in two stages. In the first stage, the linear buckling analysis was done to obtain the buckling load and mode shapes. In the second stage, the buckling mode shapes were utilized to apply geometric imperfections to perform non-linear analysis, where the material non-linearity was accounted for. The mesh size of the specimens was chosen as two times the thickness of the specimens based on the mesh convergence study (Shabhari et al. 2024). All the specimens were modelled with sharp corners at all the junctions to reduce the computational time since the curved corners are less significant for buckling analysis but increase element count resulting in higher computational time. Finer meshes were made in the location around the perforation to enable a smooth transition of stresses at the perforation corners as shown in Fig. 9. The imperfection factor was varied between 0.001 to 3 times thickness including $0.34\times t$ (Schafer and Peköz 1998) and $0.34t\sqrt{\lambda_L}$ (Walker 1975) and the ultimate capacities were obtained from the non-linear analyses to compare with the experimental results. The fixed boundary conditions were imposed on the ends of the specimens using MPC beam constraints, through the reference points located at the center of gravity as shown in Fig. 10. Hence, only the axial translation at the loading end was permitted while all other translations and rotations were constrained.

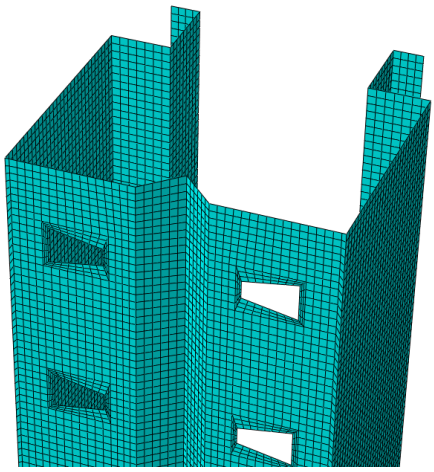

Figure 9: Meshed specimen

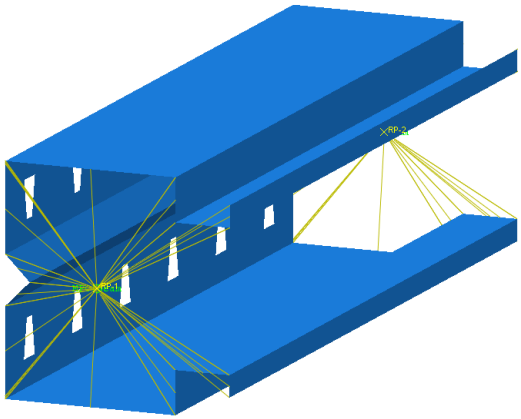

Figure 10: MPC Beam constraint for fixed support

Due to the variability in imperfection among the tested specimens, the capacity of each specimen closely aligned with experimental results with different imperfection amplitudes, ranging from 0.001 to 3 times the thickness. Based on the consolidated results presented in Table 4, the average imperfection factor of 0.8 times the thickness, with a Mean of 1.0 and a Standard Deviation of 0.08, appears to be most suitable for the tested specimens.

Table 4: Comparison of numerical results with test results

Specimen	λ_L	$P_{ul,FEA} / P_{ul,Test}$			$P_{nl,DSM} / P_{ul,Test}$
		$0.34\times t$	$0.8\times t$	Walker	
SR - G	1.00	1.02	0.96	1.02	0.99
SR - P	0.98	1.10	1.04	1.15	1.05
LR - G	0.88	1.11	1.04	1.13	1.18
LR - P	0.91	1.00	0.93	1.02	1.03
WSSR - G	1.01	0.90	0.86	0.91	0.86
WSSR - P	1.00	1.21	1.15	1.25	1.13
WSLR - G	0.88	1.02	0.96	1.03	1.06
WSLR - P	0.92	1.15	1.09	1.17	1.17
	Mean	1.06	1.00	1.08	1.06
	St. Dev.	0.09	0.08	0.10	0.10

The failure modes captured from the numerical analysis were found in agreement with the test results as shown in Fig. 11 and Fig. 12 for LR – P and WSLR – G respectively. The local buckling of the web was predominant for the specimens without web stiffener and in flanges for the specimens with web stiffener. The axial load vs shortening curves from the test and FE results for the typical specimens are shown in Fig. 13.

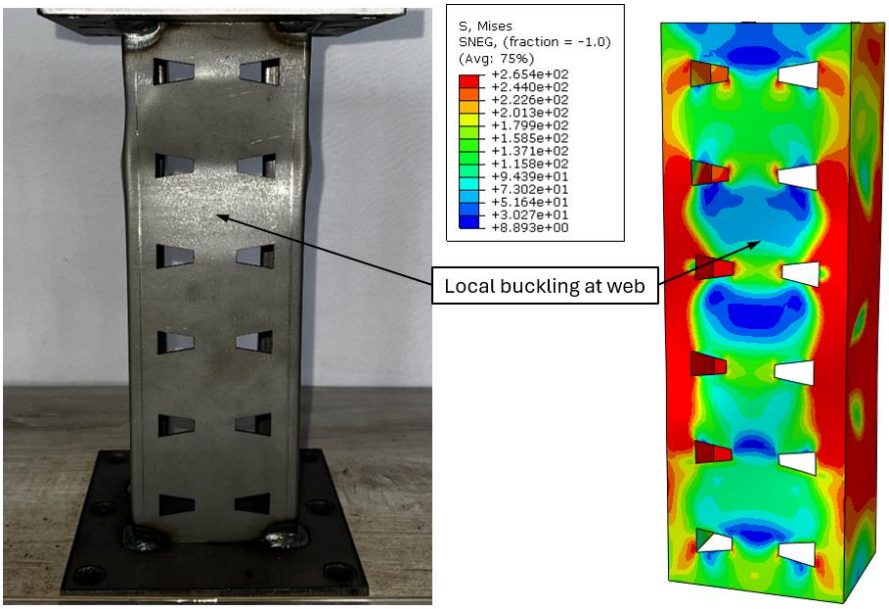

Figure 11: Comparison of numerical failure mode with test data (LR - P)

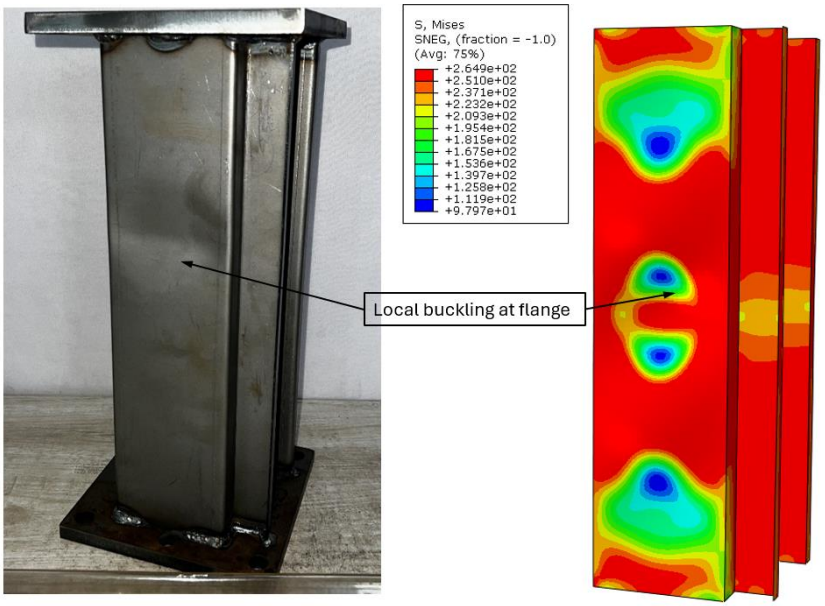

Figure 12: Comparison of numerical failure mode with test data (WSLR - G)

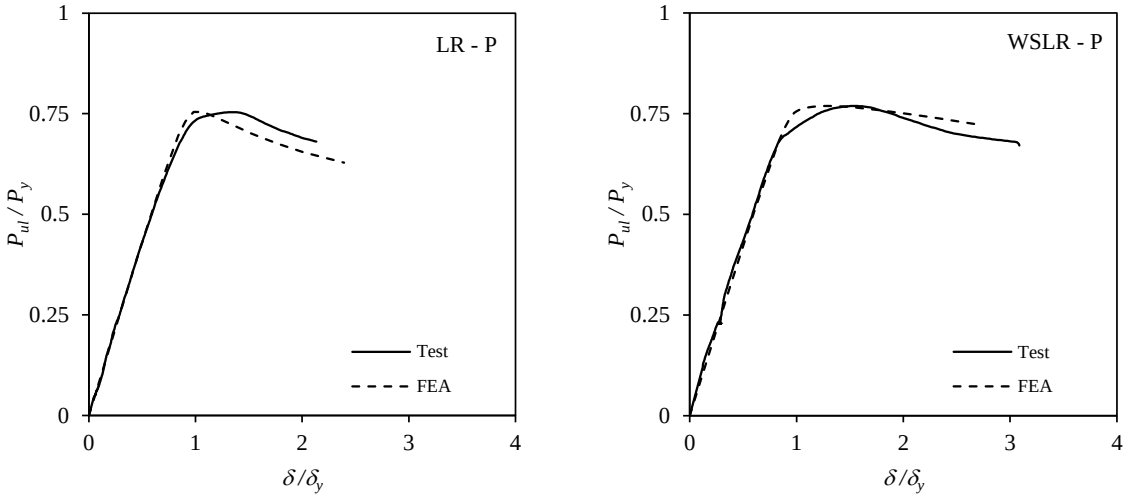

Figure 13: Normalised load vs axial shortening graphs

4.2 Parametric study

The validated numerical model was utilized to perform an extensive parametric study. A total of 1176 finite element models were analyzed, including both linear and non-linear analyses. The specimens comprise unperforated and perforated columns, categorized into the simple rack (SR), lipped rack (LR), web-stiffened simple rack (WSSR), and web-stiffened lipped rack (WSLR) geometries, with a wide range of web-to-flange ratio (aspect ratio), non-dimensional local buckling slenderness ratio (λ_L) and various shape, size, and internal angle of web stiffeners. For this study, the perforation shape was idealized as a square with 20 mm × 20 mm size having the perforation area of 400 mm^2 per perforation.

The details of the parameters and their levels are listed in Table 5 which were selected to cover a wide range of cross-sections that may be used in industrial applications. All the combinations of the factors in Table 5 were achieved by preliminary numerical analysis. For all the specimens, the web size (h) was chosen commonly as 100 mm, and the rear flanges (b_r) were chosen as half of the flange (b_f) dimensions. The flange stiffener (d_f) and lip (d) were chosen

effectively to restrain the distortional buckling. The thickness of the cross-section was varied to achieve various non-dimensional local buckling slenderness ratios (λ_L).

All the specimens were designed to fail only by local buckling to avoid the interaction of distortional and global buckling modes. Hence, a special boundary condition was employed to suppress the global buckling mode, particularly for specimens with *h/b* = 3, where the flexural buckling about the non-symmetric axis may interact with the local buckling at the post-buckling region. This technique was successfully adopted by Kumar and Kalyanaraman (2013) and Shabhari et al. (2024), without affecting the local buckling capacity of the columns. Whereas the distortional buckling was rationally excluded by choosing appropriate cross-section dimensions. Further, the rack sections are provided with flange stiffeners and rear flanges, and the columns are short, the distortional buckling strength is substantially higher than the local buckling strength resulting in the absence of distortional buckling mode. The imperfection factor suggested by Walker (1975), given as $0.3t\sqrt{\lambda_L}$, was adopted in the parametric study which was observed as more accurate across the entire range of non-dimensional slenderness ratios (λ_L), particularly advantageous for the lower values of λ_L (Shabhari et al. 2024). The various cross-sections accounted in the parametric study with variations in web stiffener shapes, sizes, and angles are shown in Fig. 14 - Fig. 16. The notation "*a*" is marked in the figures to indicate the dimension which is constant while varying other parameters. It is to be noted that when the web stiffener shape is varied, the total perimeter of the web stiffener is also kept constant.

Table 5: Parameters and their levels

Parameters	Levels	Denoted symbols
h/b	1, 2, 3	*h/b*
λ_L	0.5 to 3	λ_L
Shape of web stiffener	Triangular (V), Rectangle (R), Trapezoid (T)	*V, T, R*
Size of web stiffener	5 mm, 15 mm, 25 mm	S5, S15, S25
Angle of web stiffener	15º, 30°, 45º, 60°, 75º	A15, A30, A45, A60, A75

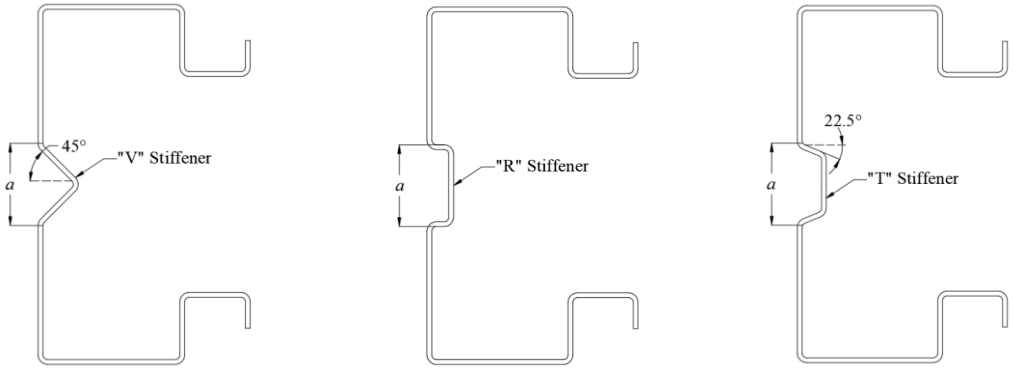

(a) (b) (c)

Figure 14: Different shapes of web stiffener

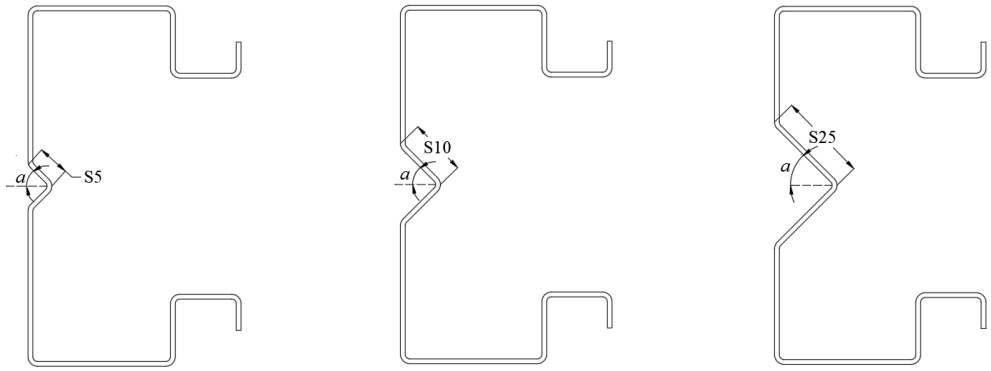

(a) (b) (c)

Figure 15: Different sizes of web stiffener

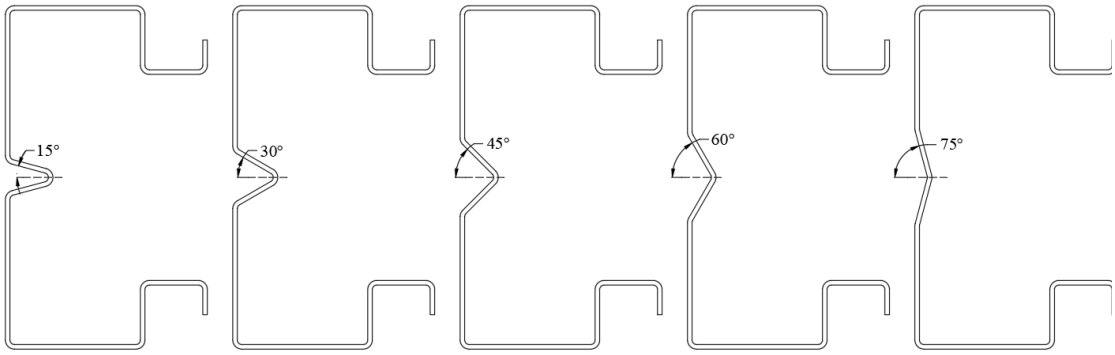

(a) (b) (c) (d) (e)

Figure 16: Different angles of web stiffener

4.2.1 Effect of web stiffener in simple and lipped rack sections

Table 6 lists the normalized ultimate capacity (P_{ul} / P_y) and the percentage increase in P_{ul} / P_y due to the web stiffener for perforated and unperforated SR, WSSR, LR, and WSLR sections. For the representation and comparison of percentage increase in ultimate capacity of both unperforated and web perforated with or without web stiffener, the results are represented using gross unstiffened cross-section's non-dimensional local buckling slenderness ratio (λ_L) as shown in Table 6. However, the actual λ_L of every cross-section are appropriately accounted in all strength calculations and can differ from the presented λ_L. The intention is to compare the percentage change in material utilization (P_{ul} / P_y) when the same cross-section is provided with the web perforation and the web stiffener. The results show that the presence of web stiffeners has significantly increased the capacity of simple and lipped racks irrespective of the web perforation. However, the effectiveness of the web stiffener reduces for lower non-dimensional local buckling slenderness ratios (λ_L). This is because the cross-section with very low λ_L would fail by yielding rather than by local buckling. Hence, with lower λ_L, the cross-section reaches its maximum material capacity at failure and consequently, the addition of web stiffeners would no longer increase its normalized capacity. In contrast, the percentage increase in P_{ul} / P_y is much higher (up to 32%) for the cross-sections with higher λ_L. Therefore, the addition of web stiffener is most beneficial for cross-sections with moderate to higher λ_L. Further, the percentage increase in (P_{ul} / P_y) is slightly lesser for the sections with web perforations when compared with the sections without perforations. For the perforated members, the stress concentration due to perforations with the interaction to local buckling failure results in a relatively lower percentage increase in normalized capacity when the web stiffener is added.

Table 6: Percentage (%) increase in P_{ul} / P_y due to the presence of web stiffeners

h/b	λ_L	P_{ul} / P_y											
		SR						LR					
		Unperforated			Perforated			Unperforated			Perforated		
		SR	WSSR	% increase	SR	WSSR	% increase	LR	WSLR	% increase	LR	WSLR	% increase
1	3.0	0.46	0.58	25.83	0.44	0.53	19.07	0.52	0.64	22.87	0.51	0.57	21.77
	2.5	0.51	0.65	26.94	0.49	0.59	20.30	0.61	0.74	22.44	0.56	0.74	32.93
	2.0	0.59	0.73	24.30	0.58	0.64	11.68	0.68	0.81	20.49	0.66	0.81	22.12
	1.5	0.72	0.86	19.81	0.69	0.78	12.92	0.76	0.89	16.99	0.84	0.84	0.04
	1.0	0.90	0.98	8.23	0.82	0.86	5.33	0.90	0.98	9.01	0.84	0.87	3.93
	0.75	0.96	0.99	3.66	0.85	0.87	2.32	0.96	0.99	3.93	0.87	0.89	2.25
	0.5	1.00	1.00	0.03	0.88	0.88	0.25	0.99	0.99	0.57	0.89	0.89	0.09
2	3.0	0.59	0.74	25.06	0.62	0.75	20.62	0.61	0.74	19.67	0.62	0.78	25.44
	2.5	0.66	0.83	26.59	0.69	0.71	3.19	0.72	0.85	17.50	0.74	0.82	10.88
	2.0	0.76	0.96	27.47	0.73	0.82	11.99	0.77	0.93	21.42	0.76	0.84	11.03
	1.5	0.80	0.99	23.91	0.73	0.83	12.91	0.80	0.98	22.59	0.76	0.85	11.58
	1.0	0.87	1.00	14.53	0.77	0.83	8.78	0.87	1.00	14.93	0.79	0.85	7.45
	0.75	0.93	1.00	7.07	0.79	0.83	4.91	0.93	1.00	7.69	0.81	0.85	4.18
	0.5	0.99	1.00	1.23	0.82	0.83	1.60	0.98	1.00	2.07	0.84	0.84	0.91
3	3.0	0.67	0.83	23.31	0.65	0.77	18.23	0.66	0.78	19.21	0.59	0.78	31.98
	2.5	0.70	0.87	25.05	0.67	0.80	19.37	0.70	0.88	26.54	0.69	0.81	16.61
	2.0	0.73	0.93	28.11	0.67	0.81	19.99	0.73	0.94	29.09	0.71	0.82	15.03
	1.5	0.77	0.98	27.80	0.71	0.81	14.88	0.76	0.98	28.80	0.74	0.83	11.88
	1.0	0.85	1.00	16.71	0.74	0.81	9.77	0.83	1.00	19.52	0.77	0.83	7.95
	0.75	0.92	1.00	8.26	0.76	0.81	6.61	0.90	1.00	10.59	0.78	0.83	5.41
	0.5	0.99	1.00	1.62	0.80	0.83	4.08	0.98	1.00	2.66	0.82	0.84	2.11

4.2.2 Effect of h/b ratio in the web stiffened cross-sections.

In this section, the effect of the *h/b* ratio in SR and LR sections with and without web stiffeners is presented. The design strengths Eq. (1) to (12) were used to compare the analytical and numerical strength predictions. The MDSM_holes and DSM_holes equations were used for the perforated cross-sections and the MDSM and DSM equations were used for unperforated sections and the results are presented in Fig. 17. The DSM and MDSM analytical predictions were accurate for all the cross-sections with very low λ_L. It shall be noted that the MDSM and MDSM_holes equations were originally formulated for lipped channel columns. Nevertheless, it also performs well for simple rack sections (Fig. 17 (a)). In the range of moderate to higher λ_L, for all other cross-sections, the MDSM_holes predictions are not accurate, but still more reliable than the DSM_holes predictions. The h/b ratio significantly influences the results, as sections with a *h/b* ratio of 1 demonstrate the lowest P_{ul} / P_y values compared to all other cross-sections without web stiffeners. This could happen because the flange experiences buckling along with the web in cross-sections with *h/b* = 1, whereas in other *h/b* ratios, the flange is significantly stockier than the web. Consequently, the post-local buckling strength may be higher causing the increased P_{ul} / P_y at higher λ_L. For the cross-sections with the stiffened web, the web is highly stiffer, and the flat width of the web is less than half of the web dimension. Hence, the simultaneous buckling of the web and flanges occurs at all the range of *h/b* ratios considered.

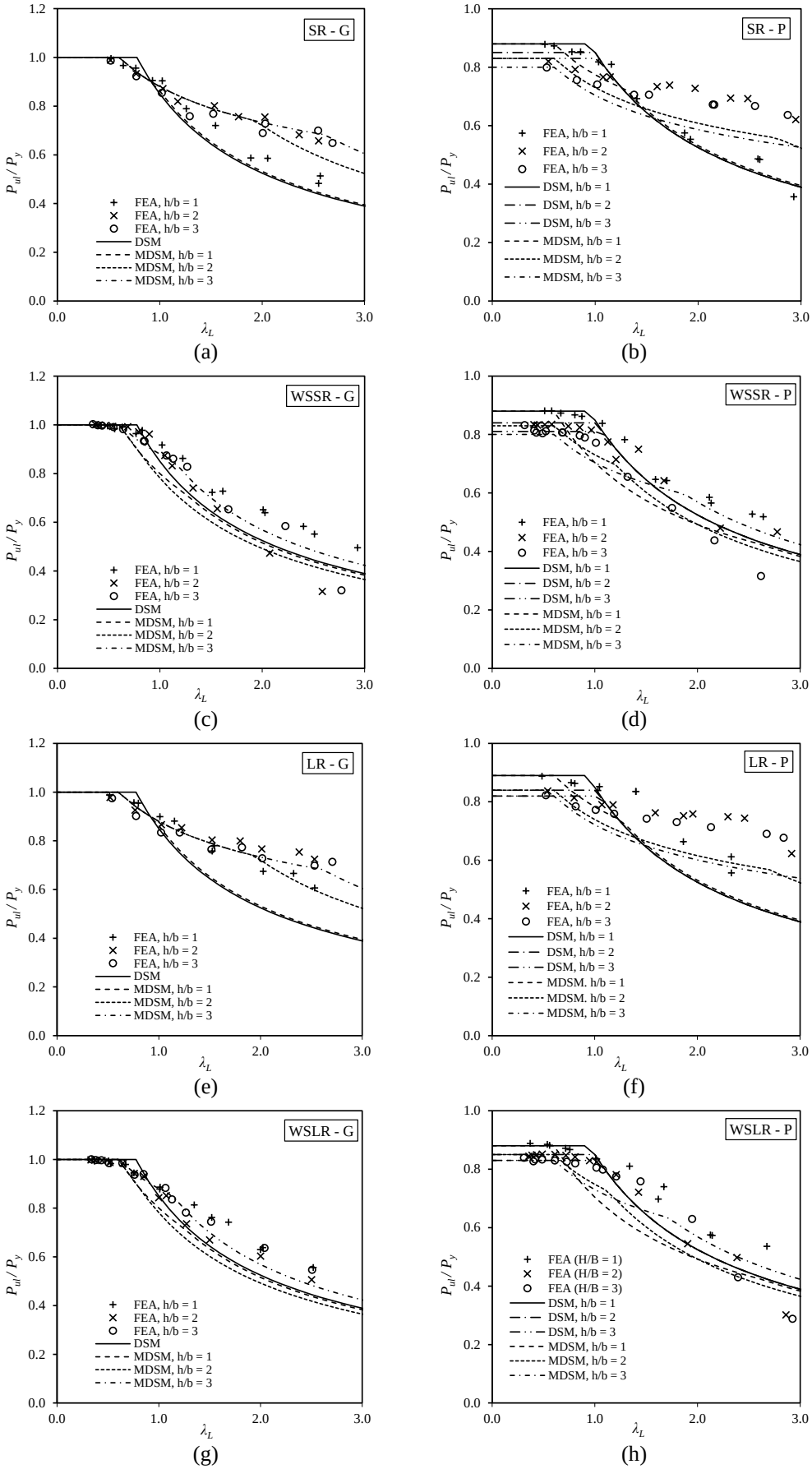

Figure 17: Effect of *h/b* ratio in rack sections

4.2.3 Effect of shape, size, and angle of the web stiffener

This section examines the influence of the shape, size, and angle of web stiffeners exclusively for the WSLR – P cross-section. The alteration in the size of the web stiffener demonstrates a significant impact on the capacity of the specimens. When the web stiffener is ineffective, the local buckling occurs across the entire width of the web (as illustrated in Fig. 18 (a)). In this case, the web stiffener is observed buckling along with the web. While the P_{ul} / P_y values for d_w = 5 are comparable to those of higher d_w within the lower to moderate λ_L range, for higher λ_L, P_{ul} / P_y values are found significantly lower because of ineffective web stiffeners, causing localized stress concentrations. In other words, the material capacity is not utilized maximum. Whereas in higher web stiffener sizes, the buckling is observed predominantly either in the net effective width of the web excluding the web stiffener or within the web stiffener. The translation of the corners of the web stiffener is not significant. Hence, the stress transfers to adjacent elements causing the stress redistribution in the entire cross sections as shown in Fig. 18 (b) & (c)). The DSM predictions are accurate in lower λ_L and reasonably safer in higher λ_L. However, it provided inaccurate and unsafe predictions for the specimens with moderate λ_L (See Fig. 19).

While comparing the shape of the stiffeners, it is evident from Fig. 20 (a) to (c), that the rectangular shape exhibited higher P_{ul} / P_y in general. However, the effect of shape is significant only for the specimens with a higher *h/b* ratio such as 3. In lower *h/b* ratios, the shape of the web stiffener is insignificant as far as the area of the cross-section is kept constant. From the results shown in Fig. 20 (b) & (c), it can be highlighted that the DSM and MDSM predictions are reasonably safe and the effect of change in the shape of the web stiffener is accounted for by λ_L as far as the perimeter of the web stiffener is not changed.

The analysis of the web stiffener angle reveals, as illustrated in Fig. 21 (a) to (c) that its impact is significant only for the rack sections with higher *h/b* ratios. In contrast, for the rack sections with lower *h/b* ratios, the P_{ul} / P_y values are nearly closer across various angles. For the sections with d_w = 5 and *h/b* = 3, all the specimens with web stiffener angle 75º failed by local buckling as the whole web was in two halfwaves in a longitudinal direction whereas the specimens with angle 15° showed local buckling at web region near the perforations. This is because the web stiffener with an angle of 15º imparts greater stiffness to the web among all the angles as the web stiffener width is constant across different angles. Still, this effect is not pronounced in the specimens with lower *h/b* ratios. The 75º web stiffener exhibits the lowest P_{ul} / P_y among all the web stiffener angles in the specimens with higher *h/b* ratios. While comparing the P_{ul} / P_y of FEA results with the DSM_holes predictions, it is evident that the λ_L fails to account for the effect of web stiffener angles causing the DSM predictions both unsafe and inaccurate.

4.3 Comparison of DSM_holes and MDSM_holes design methods

The P_{nl} / P_{FEA} results, calculated from the predictions of DSM_holes and MDSM_holes procedures are illustrated in Fig. 22 (a) to (f). The charts indicate that, across all sizes, shapes, and angles of the web stiffener, the DSM_holes and MDSM_holes predictions are similar for the specimens with higher λ_L. However, for the specimens with lower to moderate λ_L, the MDSM_holes results are more conservative and safer, while the DSM_holes predictions are less conservative and unsafe. The mean of the P_{nl} / P_{FEA} predictions of MDSM_holes is nearly equal to, but less than 1, while the mean is marginally greater than 1 in the case of DSM_holes predictions. Although the MDSM_holes provides safer and conservative results, there is a necessity to enhance the design equations for a more economical design and optimal material utilization of web-stiffened rack sections.

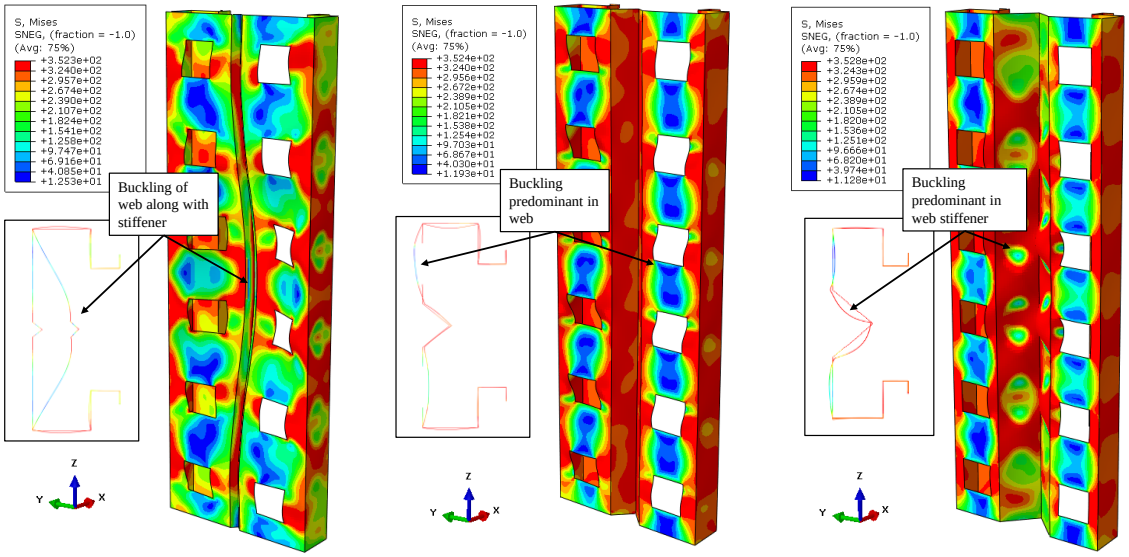

(a) Ineffective web stiffener (b) Effective web stiffener (c) Web stiffener slender than web

Figure 18: Failure modes of web-stiffened rack sections

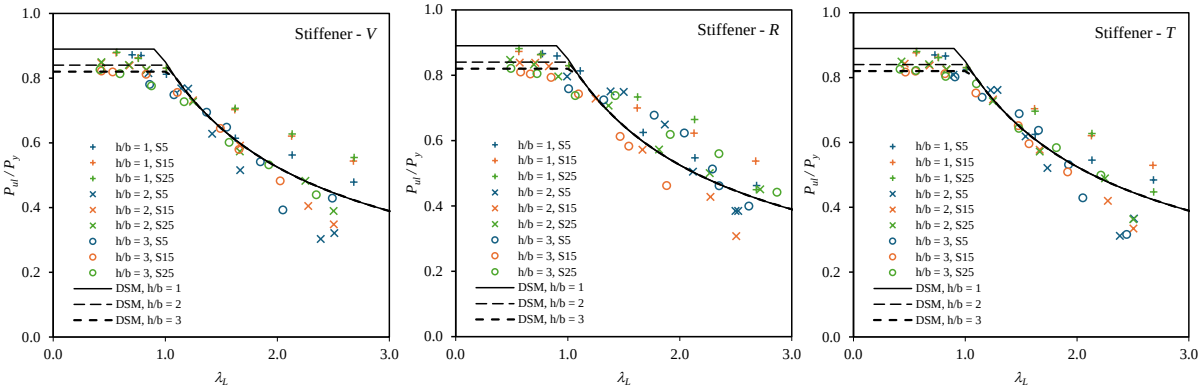

(a) (b) (c)

Figure 19: Effect of web stiffener size among various shapes of web stiffener

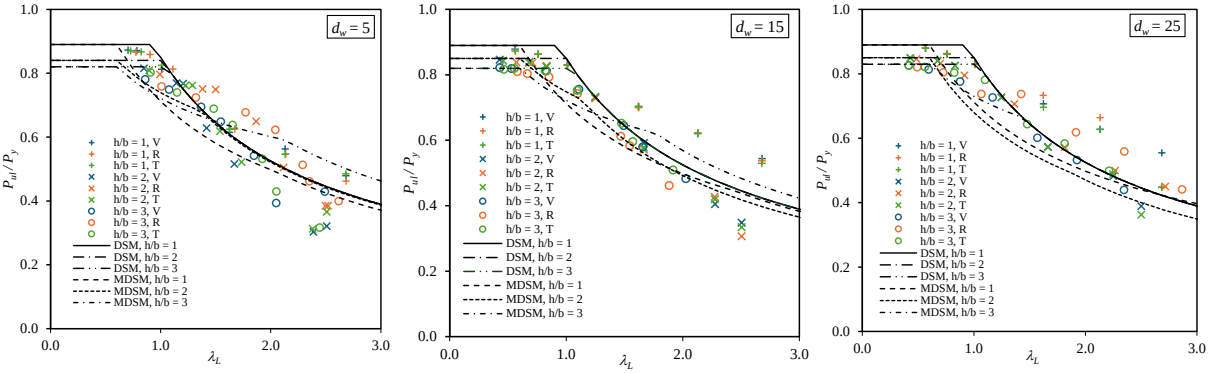

(a) (b) (c)

Figure 20: Effect of web stiffener shape in among various sizes of web stiffener

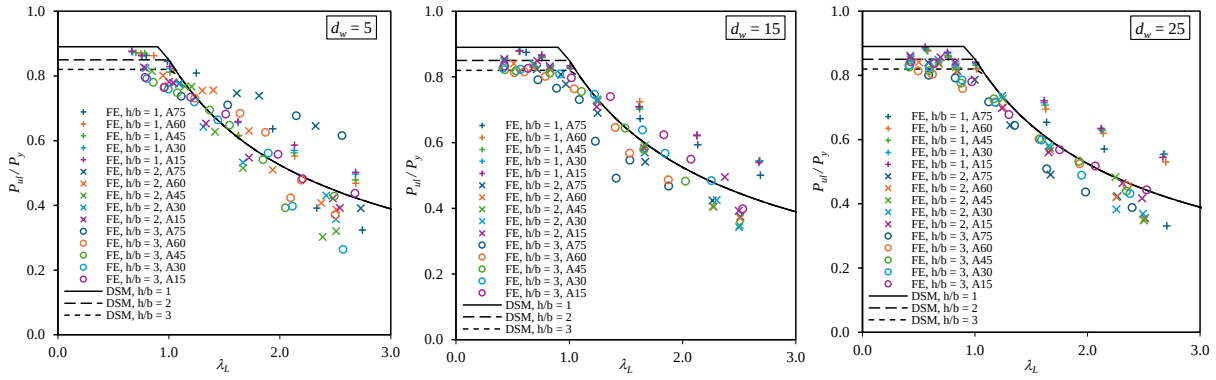

(a) (b) (c)

Figure 21: Effect of web stiffener included angle among various sizes of web stiffener

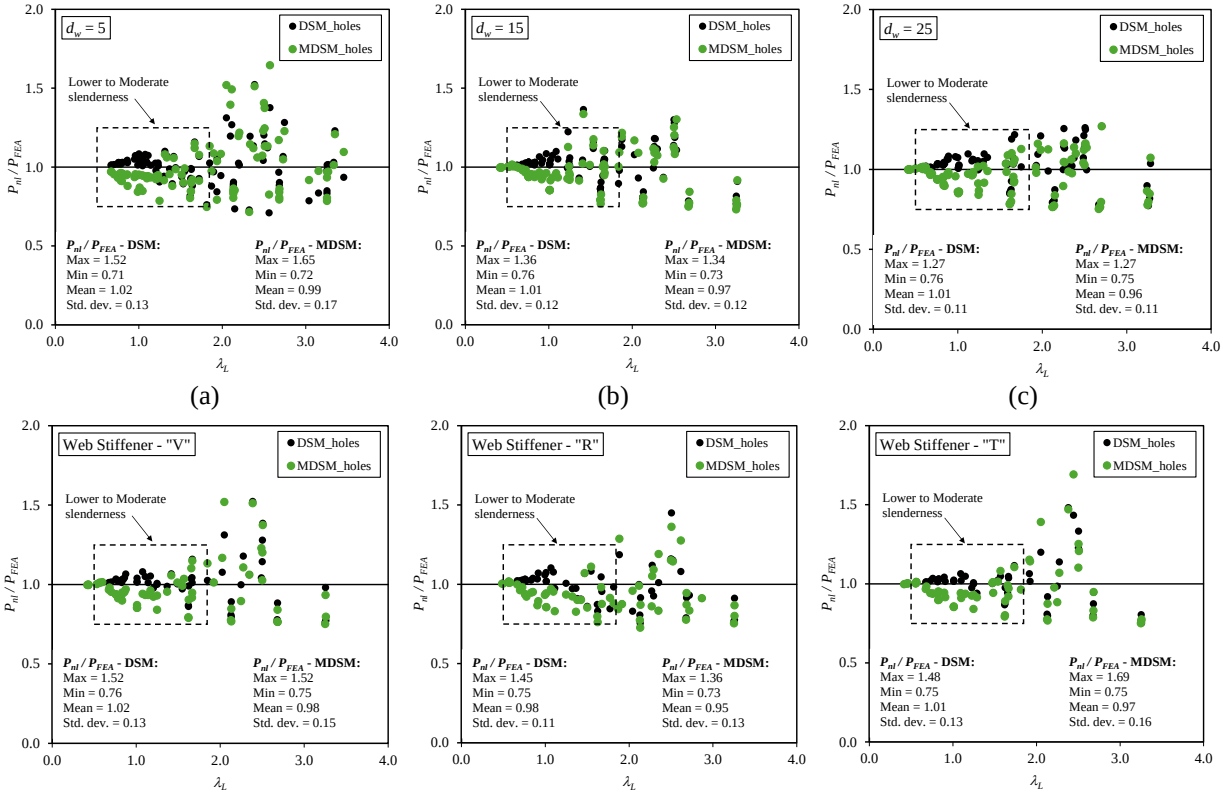

(a) (b) (c)

(d) (e) (f)

Figure 22: P_{nl} / P_{FEA} DSM and MDSM results for web stiffened perforated members

5. Conclusions

This research exemplifies the findings from experimental and numerical studies of web-perforated and web-stiffened CFS simple and lipped rack sections subjected to axial compression with fixed-end boundary conditions and failing in local buckling failure. All the columns were designed to undergo pure local buckling without any interaction of distortional or global buckling modes. A comprehensive parametric numerical investigation was performed, encompassing a wide range of *h/b* ratios, λ_L and various shapes, sizes, and angles of web stiffeners. The results indicate that the web stiffeners are effective only for the cross-sections with moderate to higher λ_L and ineffective for cross-sections with lower λ_L. The shape, size, and angle of the web stiffener are not significant for the cross-sections with lower *h/b* ratios. For specimens with higher *h/b* ratios, the size of the web stiffener plays a pivotal role in the local buckling capacity. An ineffective web stiffener could not enhance the buckling strength since it buckles as a whole web element. Adequate web stiffeners provide increased

stiffness and enhanced stress transfer across the web. The influence of the web stiffener angle in local buckling strength is not reflected in the DSM and MDSM design equations through λ_L. The local buckling strength equations need an explicit inclusion of effectiveness of web stiffener in addition to the primary parameters of aspect ratio and non-dimensional local buckling slenderness ratio. The MDSM predictions are relatively better for the unperforated rack sections. Whereas for the web perforated rack sections, the DSM_holes and MDSM_holes exhibited similar predictions for specimens with higher λ_L. The MDSM_holes predictions are more prudent and conservative for the specimens with lower to moderate λ_L. Improvements to the current DSM and MDSM local buckling strength equations are necessary for a more cost-effective design of web stiffened web perforated rack sections.

Acknowledgments
We thank M/s Craftsman Automation Ltd., Coimbatore, India, for sponsoring this research study and providing all facilities relevant to the experimental program. We would also like to thank Er. Srinivasan Ravi (CMD), Er. R Gautham Ram (Whole-Time Director), Er. D Chandrashekar (VP Design), Er. G Senthilkumar (DGM, Product Design), and Er. Amit Dhamanaskar (DGM, Static Storage Design) for their full support during the experimental investigation.

Nomenclature

A_g	-	Gross cross-sectional area
A_{net}		Net cross-sectional area
b	-	Total width of flange
b_f	-	Width of flange
b_r	-	Width of rear flange
d	-	Depth of lip
d_f	-	Depth of flange stiffener
d_w	-	Depth of web stiffener
E	-	Young's modulus
f_y	-	Yield stress
h	-	Depth of web
P_{crd}	-	Critical distortional buckling capacity
P_{cre}	-	Critical global buckling capacity
P_{crl}	-	Critical local buckling capacity
P_{nd}	-	Nominal distortional buckling capacity
P_{ne}	-	Nominal global buckling capacity
P_{nl}	-	Nominal local buckling capacity
P_y	-	Squash load (Yield load)
$P_{y,net}$	-	Squash load corresponding to net area
t	-	thickness of element
λ_D	-	Non-dimensional distortional buckling slenderness ratio
λ_e	-	Non-dimensional global buckling slenderness ratio
λ_L	-	Non-dimensional local buckling slenderness ratio

References

AISI S100. (2016). *North American Specification for the Design of Cold-Formed Steel Structural Members*. Washington DC.

ASTM E8/E8M-16a. (2016). *E8 Standard Test Methods for Tension Testing of Metallic Materials*. West Conshohocken, USA: ASTM International.

Baldassino, N., C. Bernuzzi, A. di Gioia, and M. Simoncelli. (2019). "An experimental investigation on solid and perforated steel storage racks uprights." *Journal of Constructional Steel Research*, 155 409–425. Elsevier Ltd. https://doi.org/10.1016/j.jcsr.2019.01.008.

BS EN 15512:2020. (2020). *Steel static storage systems - Adjustable pallet racking systems - Principles for structural design*. CEN-CENELEC Management Centre, Brussels.

Camotim, D., A. D. Martins, P. B. Dinis, B. Young, M. Chen, and A. Landesmann. (2020). "Mode interaction in cold-formed steel members: state-of-art report." *Steel Construction*, 13 (3) 186–207. https://doi.org/10.1002/stco.202000044.

Chen, M.-T., B. Young, A. D. Martins, D. Camotim, and P. B. Dinis. (2020). "Experimental investigation on cold-formed steel stiffened lipped channel columns undergoing local-distortional interaction." *Thin-Walled Structures*, 150 106682. https://doi.org/10.1016/j.tws.2020.106682.

Francis, R., A. Shabhari, D. Chandrasekar, and J. Vijaya Vengadesh Kumar. (2024). "Investigation of local buckling behavior of web perforated plain channel stub columns." *Journal of Constructional Steel Research*, 222 108978. Elsevier Ltd. https://doi.org/10.1016/j.jcsr.2024.108978.

Huang, L., W. Yang, T. Shi, and J. Qu. (2021). "Local and distortional interaction buckling of cold-formed thin-walled high strength lipped channel columns." *International Journal of Steel Structures*, 21 (1) 244–259. https://doi.org/10.1007/s13296-020-00436-z.

Kalyanaraman, V. (1979). "Local buckling of cold-formed steel members." *Journal of the Structural Division*, 105 (5) 813–828. https://doi.org/10.1061/JSDEAG.0005139.

Kumar, M. V. A., and V. Kalyanaraman. (2013). "Design Strength of Locally Buckling Stub-Lipped Channel Columns." 138 (11) 1291–1299. https://doi.org/10.1061/(ASCE)ST.1943-541X.0000575.

Kwon, Y. B., and G. J. Hancock. (1992). "Tests of cold-formed channels with local and distortional buckling." *Journal of Structural Engineering*, 118 (7) 1786–1803. https://doi.org/10.1061/(asce)0733-9445(1992)118:7(1786).

Kwon, Y. B., B. S. Kim, and G. J. Hancock. (2009). "Compression tests of high strength cold-formed steel channels with buckling interaction." *Journal of Constructional Steel Research*, 65 (2) 278–289. Elsevier Ltd. https://doi.org/10.1016/j.jcsr.2008.07.005.

Loughlan, J., N. Yidris, and K. Jones. (2012). "The failure of thin-walled lipped channel compression members due to coupled local-distortional interactions and material yielding." *Thin-Walled Structures*, 61 14–21. Elsevier. https://doi.org/10.1016/j.tws.2012.03.025.

Martins, A. D., D. Camotim, P. B. Dinis, and B. Young. (2015). "Local-Distortional Interaction in Cold-formed Steel Columns: Mechanics, Testing, Numerical Simulation and Design." *Structures*, 4 38–57. Elsevier B.V. https://doi.org/10.1016/j.istruc.2015.10.005.

Moen, C. D., and B. W. Schafer. (2011). "Direct Strength Method for design of cold-formed steel columns with holes." *Journal of Structural Engineering*, 137 (5) 559–570. https://doi.org/10.1061/(ASCE)ST.1943-541X.0000310.

Nedelcu, M. (2014). "Buckling mode identification of perforated thin-walled members by using GBT and shell FEA." *Thin-Walled Structures*, 82 67–81. Elsevier. https://doi.org/10.1016/j.tws.2014.04.005.

Neiva, L. H. de A., A. M. C. Sarmanho, V. O. Faria, F. T. de Souza, and J. A. B. Starlino. (2018). "Numerical and experimental analysis of perforated rack members under compression." *Thin-Walled Structures*, 130 176–193. Elsevier Ltd. https://doi.org/10.1016/j.tws.2018.05.024.

Pu, Y., M. H. R. Godley, R. G. Beale, and H. H. Lau. (1999). "Prediction of Ultimate Capacity of Perforated Lipped Channels." *Journal of Structural Engineering*, 125 (5) 510–514. https://doi.org/10.1061/(ASCE)0733-9445(1999)125:5(510).

Schafer, B. W. (2002). "Local, distortional, and Euler buckling of thin-walled columns." *Journal of Structural Engineering*, 128 (3) 289–299. https://doi.org/10.1061/(ASCE)0733-9445(2002)128:3(289).

Schafer, B. W., and T. Peköz. (1998). "Computational modeling of cold-formed steel: Characterizing geometric imperfections and residual stresses." *Journal of Constructional Steel Research*, 47 (3) 193–210. https://doi.org/10.1016/S0143-974X(98)00007-8.

Shabhari, A., V. V. K. Jeyapragasam, and D. Chandrasekar. (2024). "Local buckling behaviour of web perforated cold-formed steel lipped channel columns." *Thin-Walled Structures*, 205 112448. Elsevier Ltd. https://doi.org/10.1016/j.tws.2024.112448.

Smith, F. H., and C. D. Moen. (2014). "Finite strip elastic buckling solutions for thin-walled metal columns with perforation patterns." *Thin-Walled Structures*, 79 187–201. https://doi.org/10.1016/j.tws.2014.02.009.

Vijayavengadesh Kumar, J., and S. Arul Jayachandran. (2016). "Experimental investigation and evaluation of

Direct Strength Method on beam-column behavior of uprights." *Thin-Walled Structures*, 102 165–179. Elsevier. https://doi.org/10.1016/j.tws.2016.01.018.

Walker, A. C. (1975). *Design and Analysis of Cold-Formed Sections*. Intertext [for] the Cold Rolled Sections Association.

Yao, Z., and K. J. R. Rasmussen. (2017). "Perforated Cold-Formed Steel Members in Compression. II: Design." *Journal of Structural Engineering*, 143 (5) 1–13. https://doi.org/10.1061/(ASCE)ST.1943-541X.0001636.

Young, B., and K. J. R. Rasmussen. (1998). "Design of lipped channel columns." *Journal of Structural Engineering*, 124 (2) 140–148. https://doi.org/10.1061/(asce)0733-9445(1998)124:2(140).

Young, B., N. Silvestre, and D. Camotim. (2013). "Cold-formed steel lipped channel columns influenced by local-distortional interaction: strength and DSM design." *Journal of Structural Engineering*, 139 (6) 1059–1074. https://doi.org/10.1061/(asce)st.1943-541x.0000694.

Zhang, P., and M. S. Alam. (2022). "Compression tests of thin-walled cold-formed steel columns with Σ-shaped sections and patterned perforations distributed along the length." *Thin-Walled Structures*, 174 109082. https://doi.org/10.1016/j.tws.2022.109082.

Zhang, P., and M. S. Alam. (2023). "Assessment of buckling strength curves in Direct Strength Method for estimating axial strengths of Cold-formed Steel members considering average yield stresses of cross-sections." *Thin-Walled Structures*, 188 110823. Elsevier Ltd. https://doi.org/10.1016/j.tws.2023.110823.

Zhao, X., C. Ren, and R. Qin. (2017). "An experimental investigation into perforated and non-perforated steel storage rack uprights." *Thin-Walled Structures*, 112 159–172. Elsevier. https://doi.org/10.1016/j.tws.2016.11.016.